reaction mixture was stirred at 0 °C for 6 h to give a yellow-amber solution of **9**.

Reaction of 9: With Sodium Dimethyl Malonate (Procedure A) (20-min Reaction Time by Using 3 mmol of Sodium Dimethyl Malonate Instead of 6 mmol). Isolation by preparative layer chromatography (5:3 hexane–ethyl acetate, R_f 0.39) gave 226 mg (35%) of methyl 2-carbomethoxy-4-methylene-5-oxohexanoate: NMR (CCl_4) δ 2.23 (s, 3, CH_3CO), 2.70 (d, J = 8 Hz, 2, $CH_2CH(COOMe)_2$), 3.43 (t, J = 8 Hz, 1, $CH_2CH(COOMe)_2$), 3.60 (s, 6, $COOCH_3$), 5.72 and 5.88 (2s, 2, CH_2=C); IR (CCl_4) 1750 (ester C=O), 1732 (ester C=O), 1678 (ketone C=O) cm^{-1}. Analytically pure sample was obtained by further preparative gas chromatography (SE-30, 180 °C, retention time 7 min). Anal. ($C_{10}H_{14}O_5$) C, H.

In addition, dimethyl 2,6-dicarbomethoxy-4-acetylheptanedioate, a Michael addition product (R_f 0.19, 141 mg, 14%), was obtained: NMR (CCl_4) δ 2.16 (s, 3, CH_3CO), 1.30–2.90 (m, 5, $CH_2CH(COCH_3)CH_2$), 3.31 (t, J = 7 Hz, 2, $CH(COOMe)_2$), 3.66 and 3.70 (2 s, 12, $COOCH_3$); IR (neat) 1750–1710 (ester and ketone C=O), cm^{-1}; mass spectrum, calcd for $C_{15}H_{22}O_9$, m/e 346.1264 (M^+) missing; 315.1080 ($M^+ - CH_3O$), found 315.1075; 303.1080 ($M^+ - CH_3CO$), found 303.1090; 215.0192 ($M^+ - CH(COOCH_3)_2$), found 215.0915.

Reaction of Hybridocobalt Tetracarbonyl with Butadiene and Dimethyl Malonate. Wet $NaCo(CO)_4$ (3 mmol) in 4.4 mL of THF was added to a flask containing THF (25 mL). The flask was cooled to 0 °C. HCl gas (75 mL at 24 °C, 3.08 mmol) was added by syringe and stirred for 0.5 h to give a light yellow-green solution and white precipitate. Butadiene was contacted for 0.5 h at 0 °C and then 10 min at 25 °C to give a dark amber solution. Then the anion of dimethyl malonate (6 mmol) in 12 mL of THF was added at 25 °C under CO to give a light red solution immediately. The red color faded into light amber (~5 min). After 1 h, the mixture was shaken with saturated NH_4Cl solution. The organic layer was separated. Iodine in ether was added to decompose any cobalt carbonyl species. Excess I_2 was removed by washing with aqueous $Na_2S_2O_3$ solution. The organic layer was dried over $MgSO_4$.

NMR spectrum of the crude products indicated the formation of methyl 2-carbomethoxy-*trans*-4-hexenoate (35% based on the Co). There is no indication of the formation of methyl 2-carbomethoxy-3-methyl-4-pentenoate.

Reaction of 3 with Sodium Dimethyl Malonate in the Presence of Triphenylphosphine (Procedure B). The solution of **3** was transferred by needlestock into a 100-mL airless flask containing triphenylphosphine (0.786 g, 3 mmol). The reaction foamed, and the mixture was stirred for 20 min to give a red-orange solution. Then sodium dimethyl malonate (6 mmol) in 12 mL of THF was added at room temperature under CO atmosphere. A deep red solution resulted. It was stirred for 17.5 h to give a brown-red solution. Worked up as usual, the resulting triphenylphosphine oxide was removed by column chromatography (silica gel 60–200 mesh, 5:4 hexane–ethyl acetate). Isolation by medium-pressure LC (5:3 hexane–ethyl acetate) gave 358 mg (41%) of tetramethyl ethane-1,1,2,2-tetracarboxylate.

Acknowledgement is made to the donors of the Petroleum Research Fund, administered by the American Chemical Society for support of this research.

Registry No. 1, 82545-55-9; **2**, 82545-56-0; **3**, 82554-91-4; **4**, 82554-92-5; **5**, 82554-93-6; **6**, 82554-94-7; **7**, 82554-95-8; **8**, 82554-96-9; **9**, 36485-11-7; π-allylcobalt tricarbonyl, 12144-85-3; cobalt octacarbonyl, 10210-68-1; allyl bromide, 106-95-6; diethyl allylmalonate, 2049-80-1; sodium tetracarbonylcobalt, 14878-28-5; methyl iodide, 74-88-4; sodium dimethyl malonate, 18424-76-5; tetramethyl ethane-1,1,2,2-tetracarboxylate, 5464-22-2; sodium diethyl methylmalonate, 18242-77-6; ethyl 2-methyl-2-carbethoxy-7-oxo-*trans*-4-octenoate, 82545-57-1; sodium ethyl acetoacetate, 19232-39-4; ethyl 2-acetyl-7-oxo-*trans*-4-octenoate, 82545-58-2; sodium ethyl cyanoacetate, 18852-51-2; ethyl 2-cyano-7-oxo-*trans*-4-octenoate, 82545-59-3; ethyl 2-methyl-2-cyano-7-oxo-*trans*-4-octenoate, 82545-60-6; 2,12-dioxo-7-cyano-7-carbethoxy-*trans*,*trans*-4,9-tridecadiene, 82545-61-7; potassium ethmhyl phenylacetate, 82545-62-8; lithium cyclohexanone enolate, 21300-30-1; 1-acetyl-1,3-butadiene, 2957-06-4; isoprene, 78-79-5; butadiene, 106-99-0; methyl 2-carbomethoxy-4-methyl-7-oxo-4-octenoate, 82545-63-9; methyl 2-carbomethoxy-5-methyl-7-oxo-4-octenoate, 82545-64-0; benzyl bromide, 100-39-0; ethyl 2-carbethoxy-2-methyl-7-oxo-8-phenyl-*trans*-4-atenoate, 82545-65-1; phenylacetyl chloride, 103-80-0; ethyl 2-acetyl-7-oxo-8-phenyl-*trans*-octenoate, 82545-66-2; ethyl bromoacetate, 105-36-2; methyl 2-carbomethoxy-7-oxo-8-carbethoxy-*trans*-4-octenoate, 82545-67-3; chloromethyl methyl ether, 107-30-2; ethyl 2-methyl-2-carbethoxy-*trans*-4-hexenoate, 82545-68-4; 1,3-cyclohexadiene, 592-57-4; 1-acetyl-1,3-cyclohexadiene, 53329-13-8; allene, 463-49-0; methyl 2-carbomethoxy-4-methylene-5-oxohexanoate, 82545-69-5; dimethyl 2,6-dicarbomethoxy-4-acetylheptanedioate, 82545-70-8; dimethyl malonate, 108-59-8; methyl 2-carbomethoxy-*trans*-4-hexenoate, 82545-71-9.

Kinetics and Mechanism of the Stepwise Dissociation of Iron(III) from Ferrioxamine B in Aqueous Acid

Bruce Monzyk and Alvin L. Crumbliss*

Contribution from the Department of Chemistry, P. M. Gross Chemical Laboratory, Duke University, Durham, North Carolina 27706. *Received August 21, 1981*

Abstract: Deferriferrioxamine B (H_3DFB) is a linear trihydroxamic acid siderophore with molecular formula $NH_2(CH_2)_5[N(OH)C(O)(CH_2)_2C(O)NH(CH_2)_5]_2N(OH)C(O)CH_3$. In aqueous solution at pH 5, the siderophore forms a hexadentate chelate with iron(III), ferrioxamine B ($Fe(HDFB)^+$), in which the terminal amine group is protonated. The aquation reaction of ferrioxamine B has been investigated over the $[H^+]$ range 0.03–1.0 M at 25.0 °C and ionic strength 2.0 ($NaClO_4/HClO_4$). The dissociation reaction, which may be represented as $Fe(HDFB)^+ + 3H_{aq}^+ \rightleftharpoons Fe_{aq}^{3+} + H_4DFB^+$, is observed to proceed in four kinetically distinguishable stages. The microscopic rate constants for the first three steps are 2.9×10^2 s^{-1}, 1.4×10^1 s^{-1}, and 1.8×10^{-1} s^{-1}. The final dissociation step proceeds by parallel $[H^+]$-dependent and $[H^+]$-independent paths, with rate constants of 1.9×10^{-3} M^{-1} s^{-1} and 2.1×10^{-3} s^{-1}, respectively. Equilibrium quotients have also been determined for various stages of the reaction. Ferrioxamine B formation rate constants are computed to be 2×10^{-1} M^{-1} s^{-1} and 2×10^2 M^{-1} s^{-1} for the reactions of H_4DFB^+ with $Fe(H_2O)_6^{3+}$ and $Fe(H_2O)_5OH^{2+}$, respectively. Five intermediate species between fully coordinated reactant and completely dissociated products are detectable by spectral and/or kinetic techniques. A mechanism is proposed whereby the intermediates correspond to the stepwise unwrapping of deferriferrioxamine B from iron(III), starting with the N–O oxygen atom at the protonated amine end of the linear trihydroxamic acid ligand. Careful analysis of the aquation reaction suggests that the detailed mechanism for mono(hydroxamato)iron(III) dissociation is applicable to the dissociation of each hydroxamate group of deferriferrioxamine B, including the important role of coordinated H_2O cis to the dissociating hydroxamate group, acid dependencies, and the role of the hydroxamate group in the transition state of the dissociating complex. The importance of mechanistic information for iron release from ferrioxamine B in understanding siderophore-mediated iron transport is discussed.

Iron is an essential nutrient for microorganisms, but due to hydrolysis is insoluble at physiological conditions. Consequently, microorganisms synthesize iron(III)-specific chelating agents (siderophores) in order to solubilize iron from the environment

0002-7863/82/1504-4921$01.25/0

by complexation and transport it to the cell.[1-5] The study of the probable mechanisms for this siderophore-mediated iron-transport process is an active area of current research.[1-8] After complexation, the iron must be released by the siderophore either at the cell wall or after penetration into the cell. This release mechanism may involve iron exchange with other chelators, destruction of the siderophore ligand (e.g., hydrolysis) with subsequent release of iron, or a reduction of iron(III) to a more labile iron(II) species.

The siderophores are characterized by their high stability constants for iron(III) chelation.[1,6] Considerable information concerning iron(III)–siderophore stability constants exists in the literature, but there are a few kinetic data available for the corresponding iron(III) chelation and dissociation reactions. These kinetic data are of importance in understanding the molecular basis for iron bioavailability in microorganisms.

Ferrioxamine B (I), isolated from *Nocardia* or *Streptomyces*,

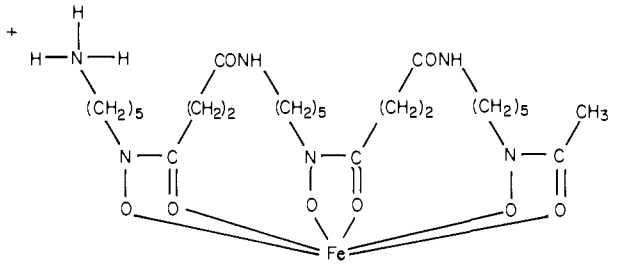

$Fe(HDFB)^+$
I, Ferrioxamine B

is a linear trihydroxamic acid siderophore coordinated to iron(III).[9] The subject of this report is the details of the kinetics and mechanism of iron dissociation from ferrioxamine B in its hexadentate chelated form to produce Fe_{aq}^{3+} and deferriferrioxamine B in acidic medium (reaction 1). The ferrioxamine B stability

$$Fe(HDFB)^+ + 3H_{aq}^+ \rightleftharpoons Fe_{aq}^{3+} + H_4DFB^+ \qquad (1)$$

constant,[10] complex formation kinetic studies at conditions different from ours,[11,12] and iron(III)-exchange kinetics between ferrioxamine B and ferrichrome A and EDTA[13] have been reported. However, a detailed kinetic study of iron dissociation from ferrioxamine B has not been made. Ligand dissociation kinetics can provide more information about the polydentate deferriferrioxamine B ligand than can formation studies, partially due to the interchange nature of the formation reaction and the fact that processes subsequent to initial bond formation are not kinetically observable. Our results also include stepwise equilibrium measurements that allow us to calculate equilibrium quotients for various steps in the dissociation reaction. Formation rate data are also calculated. A preliminary report of some of our results has been made.[14]

Although the aqueous acid medium used in this study is different from that found at physiological conditions, the results may be applicable to an understanding of the molecular basis for iron bioavailability mediated specifically by ferrioxamine B and/or to the general case of hydroxamate-based siderophores. Additional interest in the mechanism of iron binding and release by ferrioxamine B comes from its use in the iron-free form as a drug (trade name DESFERAL), which is used for the removal of iron from humans suffering from transfusion-induced iron overload (β-thalassemia).[15-18]

In addition to its biological significance, interest in the aqueous solution chemistry of high-spin iron(III) arises from the complexity of its hydrolysis reactions, its position as a representative first-row transition metal, and its industrial applications. Several reviews that include the aqueous ligand-substitution reactions of iron(III) are available.[19-21] Complex formation at Fe_{aq}^{3+} is described as an interchange process. In some cases it has been suggested that reaction at $Fe(H_2O)_6^{3+}$ proceeds by an I_a process.[22-26] In most instances it is believed that substitution reactions at $Fe(H_2O)_5OH^{2+}$ proceed via an I_d mechanism, although there are some results that support some associative character to these reactions.[23,24] Unfortunately, most of the kinetic studies of ligand substitution at Fe_{aq}^{3+} to date have been complex-formation studies. Relatively few aquation studies have been carried out.[27] It is often dissociation reaction kinetics that yield the most information about the mechanistic role of the ligands, due to the interchange nature of the complex formation. Hydroxamic acids are excellent ligands for probing the intimate mechanism of substitution at Fe_{aq}^{3+}.[24] Therefore, the results of an investigation of ferrioxamine B aquation kinetics have application to an understanding of the fundamentals of ligand-substitution processes at aqueous high-spin iron(III) and to an understanding of the molecular mechanism for iron bioavailability.

Experimental Section

Materials. Sodium perchlorate was prepared by neutralization of Na_2CO_3 (Fisher, ACS certified) by $HClO_4$ (Fisher, ACS reagent) and was recrystallized from water prior to use. All solutions were prepared by using water that was purified by distilling conductivity water from acidic $K_2Cr_2O_7$ and then slowly from basic $KMnO_4$ in an all-glass apparatus with Teflon sleeves and stopcocks. Hydrated ferric ammonium sulfate was obtained from Fisher and deferriferrioxamine B was obtained as a generous gift from Ciba-Geigy as the methanesulfonate salt.

Preparation of $[Fe(HDFB)]ClO_4 \cdot 5H_2O$. Deferriferrioxamine B (H_3DFB) (2.0 g, 3.0 mmol) as its methanesulfonate salt was dissolved in 20 mL of water, and hydrated ferric ammonium sulfate (1.5 g, 3.0 mmol) was added with stirring. The deep red color of ferrioxamine B ($Fe(HDFB)^+$) formed immediately. After stirring for 30 min, solid $NaHCO_3$ was added slowly in small portions until effervescence ceased, and

(1) Neilands, J. B. In "Inorganic Biochemistry"; Eichhorn, G., Ed.; Elsevier: New York, 1973; Chapter 5.
(2) Neilands, J. B. *Adv. Chem. Ser.* **1977**, *No. 162*, 3.
(3) Neilands, J. B. in In "Iron in Biochemistry and Medicine", 2nd ed.; Jacobs, A., Worwood, M., Eds.; Academic Press: New York, 1980; p 529.
(4) Neilands, J. B. *Annu. Rev. Biochem.* **1981**, *50*, 715.
(5) Emery, T. *Met. Ions Biol. Syst.* 1978, *7*.
(6) Raymond, K. N.; Abu-Dari, K.; Sofen, S. R. *ACS Symp. Ser.* **1980**, *119*, 133 and references therein.
(7) Raymond, K. N.; Carrano, C. J. *Acc. Chem. Res.* **1979**, *12*, 183.
(8) Raymond, K. N. *Adv. Chem. Ser.* **1977**, *No. 192*, 33.
(9) According to current convention, the term ferrioxamine B will be used to represent the iron(III) complex and deferriferrioxamine B to represent the iron-free trihydroxamic acid.
(10) Schwarzenbach, G.; Schwarzenbach, K. *Helv. Chim. Acta.* **1963**, *46*, 1390.
(11) Lentz, D. J.; Henderson, G. H.; Eyring, E. M. *Mol. Pharmacol.* **1973**, *6*, 514.
(12) Kazmi, S. A.; McArdle, J. V. "Abstracts of Papers", Second Chemical Congress of the North American Continent, Las Vegas, NV, Aug. 1980; American Chemical Society: Washington, DC; INOR 37; *J. Inorg. Biochem.* **1981**, *15*, 153.
(13) Tufano, T. P.; Raymond, K. N. *J. Am. Chem. Soc.* **1981**, *103*, 6617.
(14) Monzyk, B.; Crumbliss, A. L. *Inorg. Chim. Acta* **1981**, *55*, L5.
(15) Anderson, W. F. *ACS Symp. Ser.* **1980**, *No. 140*, 251.
(16) "Chelation Therapy in Chronic Iron Overload"; Zaino, E. C., Roberts, R. H., Eds.; Stratton: New York, 1977.
(17) "Development of Iron Chelators for Clinical Use". *HEW (U.S.) Circ.* **1977**, *no.* (NIH) 76-994.
(18) "Development of Iron Chelators for Clinical Use"; Martell, A. E., Anderson, W. F., Badman, D. G., Eds.; Elsevier North Holland: New York, 1981.
(19) Margerum, D. W.; Cayley, G. R.; Weatherburn, D. C.; Pagenkopf, G. K. In "Coordination Chemistry"; Martell, A. E., Ed.; American Chemical Society: Washington, DC, 1978; Volume 2, p 1.
(20) Wilkins, R. G. "The Study of Kinetics and Mechanisms of Reactions of Transition-Metal Complexes"; Allyn and Bacon: Boston, 1974.
(21) Basolo, F.; Pearson, R. G. "Mechanisms of Inorganic Reactions"; Wiley: New York, 1967.
(22) Swaddle, T. W. *Coord. Chem. Rev.* **1974**, *14*, 217.
(23) Gomwalk, U. D.; Lappin, A. G.; McCann, J. P.; McAuley, A. *Inorg. Chim. Acta* **1977**, *24*, 39.
(24) Monzyk, B.; Crumbliss, A. L. *J. Am. Chem. Soc.* **1979**, *101*, 6203.
(25) Grant, M.; Jordan, R. B. *Inorg. Chem.* **1981**, *20*, 55.
(26) Dodgen, H. W.; Liu, G.; Hunt, J. P. *Inorg. Chem.* **1981**, *20*, 1002.
(27) See, for example: ref 24; Nakamura, K.; Tsuchida, T.; Yamagishi, A.; Fujimoto, M. *Bull. Chem. Soc. Jpn.* **1973**, *46*, 456. Cavasino, F. P.; Di Dio, E. *J. Chem. Soc., A* **1970**, 1151. Mentasti, E. *Inorg. Chem.* **1979**, *18*, 1512.

after stirring for 1 h, the solution was filtered through a medium-sintered-glass filter funnel with suction. The reaction solution was then passed through an anion-exchange column (Bio-Rad analytical grade anion exchange resin AG1-S5 50–100 mesh; tenfold molar excess prepared in the ClO_4^- form by using 2 M $HClO_4$) followed by washing, and the solvent was removed under reduced pressure. The residue was dissolved in a few milliliters of *dry* methanol, with warming as needed. (Fresh analytical grade methanol is sufficient; however, the presence of very small amounts of water must be avoided as it causes formation of an oil in the next step). After filtering, the dark red methanolic solution was poured into a 100-fold volume excess of ethyl acetate with stirring. A pink precipitate of hydrated ferrioxamine B formed immediately as a fine dispersion, which was made to coagulate by swirling the mixture. Since the pink solid readily decomposes on a sintered-glass funnel exposed to the air, the solid was collected by centrifugation while a thin layer of solvent was maintained to cover the solid. (The mixture was easily handled by centrifuging small portions, followed by decantation of the solvent and then addition of more of the mixture.) The complex was then redissolved in methanol, filtered, added to ethyl acetate, and then collected by centrifugation several more times as described. A large volume excess of ethyl acetate was important to prevent large losses. After centrifuging for the final time, the supernatant was decanted, leaving a thin layer of solvent to cover the precipitate. The slurry was transferred to a Petri dish, and the remaining solvent was removed slowly under mild vacuum in a small vacuum desiccator. The desiccator and contents were then evacuated (10^{-3} torr) and heated in an oven at 90 °C with continuous pumping for 2 days. The final product (70% yield) was stored over P_2O_5 in a desiccator. The visible and IR spectra are the same as that reported for the chloride salt.[28] The molar absorbtivity at 425 nm (eight preparations, pH 5) is 2.46 (0.03) × 10^3 M^{-1} cm^{-1}. Anal. Calcd for $[Fe(C_{25}H_{46}O_8N_6)]ClO_4 \cdot 5H_2O$ (M_r = 803): C, 37.87; H, 6.18; N, 10.07. Found: C, 37.35; H, 7.02; N, 10.45.

Methods. Electronic spectra were obtained on a Beckman Acta III spectrophotometer equipped with a water-jacketed cell holder. Kinetic measurements were made by using an Aminco stopped-flow apparatus and digital data acquisition system described previously.[24] Dissociation kinetics were monitored at 425 nm by flowing together a solution of ferrioxamine B at the appropriate ionic strength with an aqueous solution containing the appropriate concentrations of $HClO_4$ and $NaClO_4$. All kinetic data were collected at 25.0 °C and ionic strength 2.0 ($HClO_4$/$NaClO_4$). The kinetic analysis often involved measuring a rate constant in the presence of another process with a rate constant not largely different from the one of interest. The two rate constants were determined in the usual manner of subtracting successive first-order processes.[29] This procedure was programmed into the data-reduction system previously described.[24] Absorption spectra for intermediate species were obtained by recording infinite-time absorbance values from kinetic runs for successive reactions as a function of wavelength. Data reduction for both the equilibrium and kinetic analyses required extensive use of nonlinear least-squares curve-fitting techniques. These were performed by using a standard Fortran IV program[30] adapted for use at the Triangle Universities Computational Center (TUCC). Uncertainties are reported as single standard deviations.

Results

Ferrioxamine B is completely coordinated and very stable with respect to dissociation above pH 3. Neutral refrigerated solutions are air and thermally stable for weeks. The complex is extremely soluble in water, where it produces dark red solutions when concentrated, which appear orange when dilute. Its visible spectrum is insensitive to $[H^+]$ from about 10^{-3} to at least 10^{-7} M. The color is due to a single visible absorption band with λ_{max} = 425 nm (ϵ = 2460 (30) M^{-1} cm^{-1}) (Figure 1) which is believed to be due to a ligand-to-metal charge-transfer electronic transition.

Below a pH of about 3, however, the visible spectrum of ferrioxamine B changes dramatically from that at lower acidities and is very pH dependent. Upon the addition of acid to dilute solutions (<10^{-3} M) of ferrioxamine B, the orange color changes to red. A stable color is reached only after several minutes. The spectral changes that occur when $[H^+]$ is changed from 10^{-5} to 0.5 M in a solution of ferrioxamine B are shown in Figure 1. The shift in λ_{max} toward longer wavelengths and the accompanying

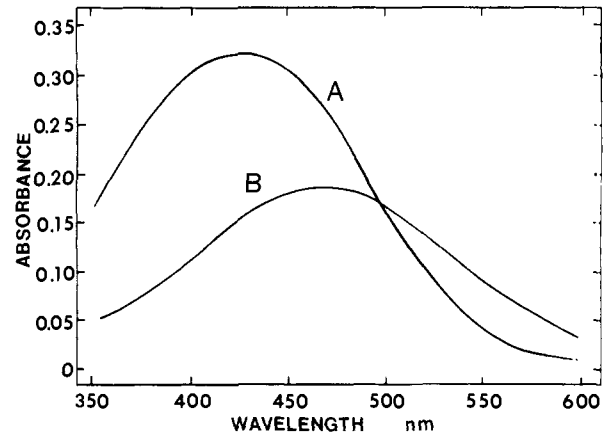

Figure 1. (A) Visible spectrum of ferrioxamine B. Conditions: $[Fe(HDFB)^+]_{tot}$ = 2.78 × 10^{-4} M; pH 5; I = 2.00 ($NaClO_4$); 25 °C. (B) Visible spectrum of ferrioxamine B after equilibration (for 10 min) with 0.5 M $HClO_4$. Conditions: $[Fe(HDFB)^+]_{tot}$ = 1.39 × 10^{-4} M; I = 2.00 ($NaClO_4$/$HClO_4$); 25 °C.

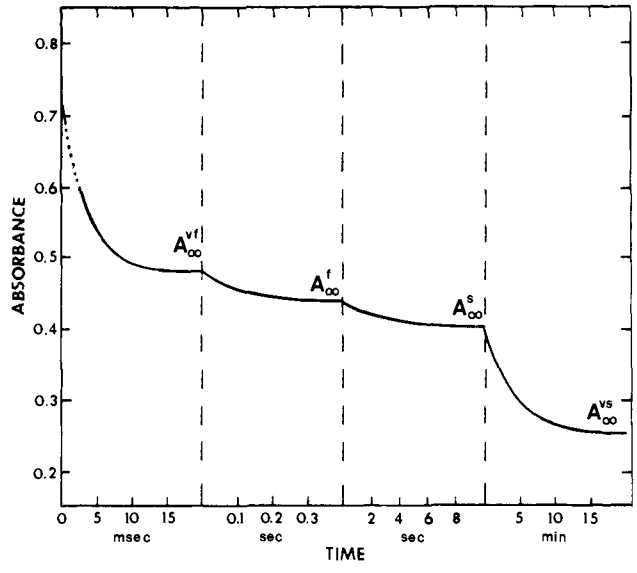

Figure 2. Illustration of the four first-order observable processes in the aquation reaction of ferrioxamine B. Conditions: 1.0 M $HClO_4$; I = 2.00 ($HClO_4$/$NaClO_4$); 25 °C; $[Fe(HDFB)^+]_{tot}$ = 2.90 × 10^{-4} M; λ = 425 nm.

decrease in absorbance are consistent with the siderophore ligand dissociating from the iron(III) center as it is replaced by coordinated water. The driving force for this dissociation reaction is the protonation of the basic N–O oxygen atoms of the hydroxamate groups at high $[H^+]$. The affinity of the siderophore for iron(III) is such that complete aquation of ferrioxamine B does not occur even in 1 M $HClO_4$. Color stability is attained in 5–10 min when the pH is dropped below 2. At high acidities (about 0.5 M or greater) a very slow bleaching reaction occurs, which has a half-life of about 1.5 days. This last reaction is not reversible, in that the color of ferrioxamine B cannot be regenerated when the pH is raised again, which suggests that ligand decomposition occurs. This final bleaching reaction was not studied further.

As Figure 2 indicates, four first-order kinetic processes are observable spectrophotometrically for the aquation of $Fe(HDFB)^+$ in acid media (Table I).[31] For convenience these four successive reactions will be referred to as the very fast, fast, slow, and very slow reactions (vf, f, s, vs), which also qualitatively describes their relative rates at our conditions. Figure 3 illustrates the pH dependence of the equilibrium position for each successive reaction. The star refers to the initial absorbance of the solution of complex

(28) Bickel, H.; Bosshardt, R.; Gäumann, E.; Reusser, P.; Vischer, E.; Voser, W.; Wettstein, A.; Zähner, H. *Helv. Chim. Acta* **1960**, *43*, 2118.
(29) Reference 20, p 24.
(30) This program fits functions to data in which parameters appear either linearly or nonlinearly by using Gauss' iterative least-squares method.
(31) See paragraph at end of paper regarding supplementary material.

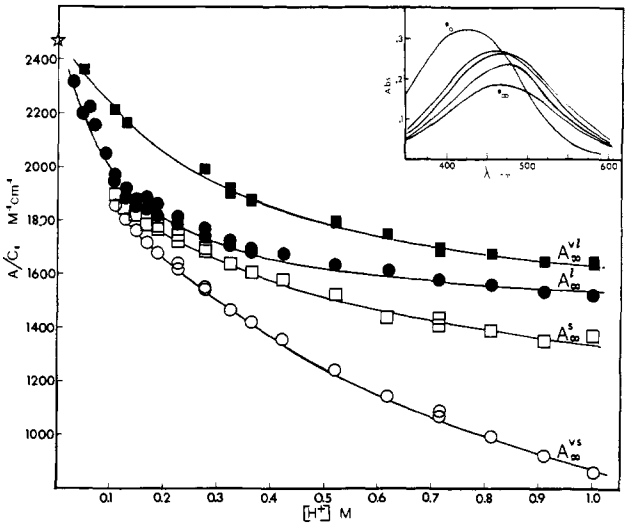

Figure 3. Illustration of the dependence of the equilibrium absorbance on the concentration of $HClO_4$ for each observable process in the aquation reaction of ferrioxamine **B**. A_∞^{vf}, A_∞^{f}, A_∞^{s}, and A_∞^{vs} represent the equilibrium absorbance measured after the very fast, fast, slow, and very slow reactions, respectively (Table I).[31] Conditions: 25.0 °C; I = 2.00 ($NaClO_4/HClO_4$); $[Fe(HDFB)^+]_{tot} = C_T = 2.90 \times 10^{-4}$ M; λ = 425 nm. Number of determinations for each absorbances = 7 (4), range 3–16. Inset shows the accompanying spectral changes at $[H^+]$ = 0.5 M, where the absorption maximum shifts smoothly from 425 to ~480 nm. t_0 represents the undissociated ferrioxamine B absorption spectrum and t_∞ the absorption spectrum corresponding to A_∞^{vs}. Intermediate spectra in order of decreasing absorbance at 425 nm correspond to A_∞^{vf}, A_∞^{f}, and A_∞^{s}. Data are from Table II.[31] Conditions are as described above.

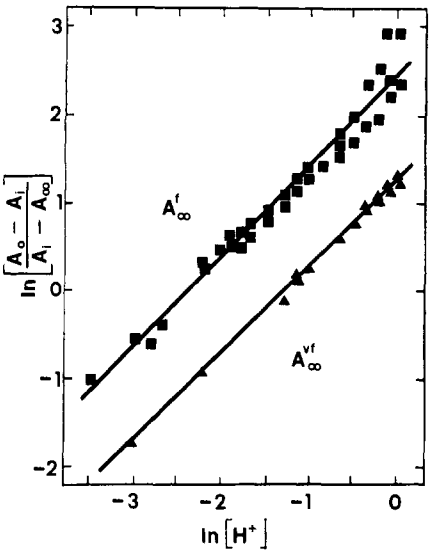

Figure 4. Determination of the number of hydrogen ions involved in the equilibria present after the very fast (A_∞^{vf} slope = 1.00) and fast (A_∞^{f} slope = 1.03) reactions. Data and conditions are from Table I.[31]

measured independently at pH 5. The inset of Figure 3 gives the visible spectrum of the reaction solution of each successive equilibrium position for the case where $[H^+]$ = 0.5 M. The spectral changes are from a maximum absorption at 425 nm, due to $Fe(HDFB)^+$ (starting material) at time zero, to a maximum absorption at ca. 480 nm, with a significant molar absorbtivity decrease after a few minutes. These spectral changes are consistent with a stepwise unwrapping of the hexadentate trihydroxamate ligand from the iron(III) center with concomitant substitution by water. In addition, a small hypsochromic shift occurs during the very slow reaction. These data are tabulated in Table II for $[H^+]$ = 0.025 and 0.5 M.[31]

The fact that the A_∞^{f}/C_T values vary at low $[H^+]$ and are roughly independent of $[H^+]$ at higher $[H^+]$ while the A_∞^{vs} values

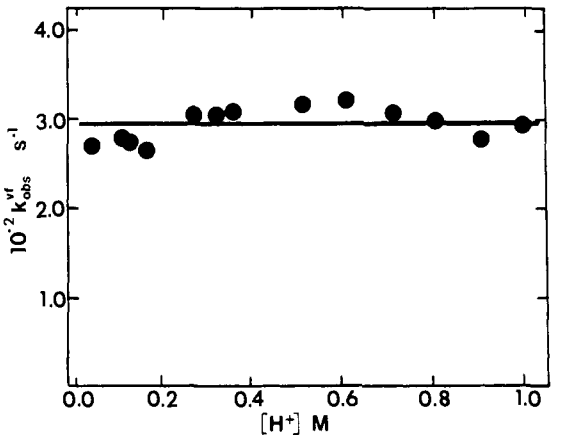

Figure 5. Observed first-order rate constant for the very fast reaction, k_{obsd}^{vf}, plotted as a function of $[H^+]$. Conditions: 25.0 °C; I = 2.0 ($NaClO_4/HClO_4$); $[Fe(HDFB)^+]_{tot} = 2.90 \times 10^{-4}$ M. Each data point represents 4–8 separate determinations. Data are from Table IV.

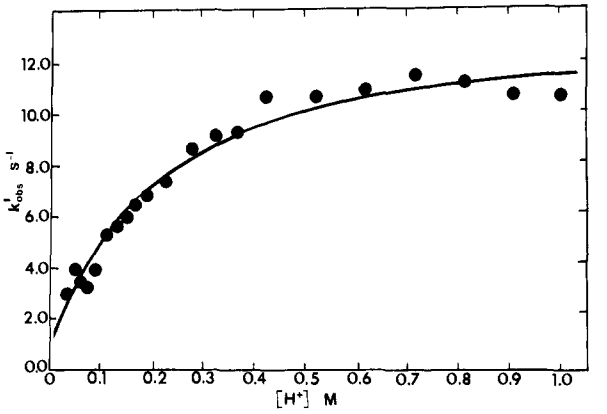

Figure 6. Observed first-order rate constant for the fast reaction, k_{obsd}^{f}, plotted as a function of $[H^+]$. Conditions are given in the legend of Figure 5. Each data point represents 3–13 separate determinations. Data are from Table IV.

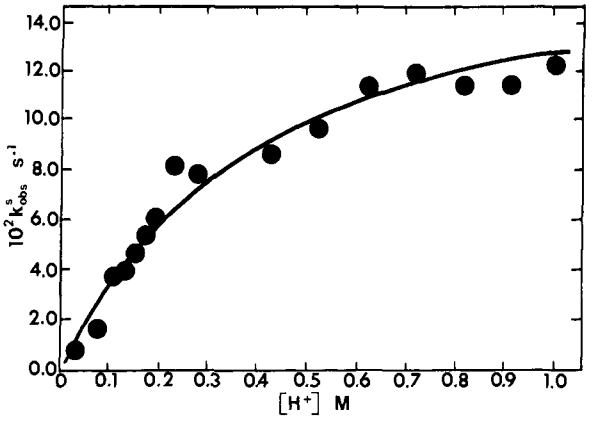

Figure 7. Observed first-order rate constant for the slow reaction, k_{obsd}^{s}, plotted as a function of $[H^+]$. Conditions are given in the legend of Figure 5. Each data point represents 2–4 separate determinations. Data are from Table IV.

remain $[H^+]$ dependent indicates that a minimum of two H_{aq}^+ ions are involved in the overall reaction.[32] That only one H_{aq}^+ ion is involved in the very fast and fast reactions is illustrated by the Hill plot shown in Figure 4, where the slope in each case is

(32) C_T represents the total $[Fe(HDFB)^+]$ and A/C_T is the apparent molar extinction coefficient ϵ_{APP}. A_∞^{vf}, A_∞^{f}, A_∞^{s}, and A_∞^{vs} represent the equilibrium absorbances measured after the very fast, fast, slow, and very slow reactions, respectively. ϵ_A, ϵ_B, ϵ_{BH}, ϵ_C, and ϵ_{CH} represent the molar extinction coefficients of the species A^+, B^+, BH^{2+}, C^{2+}, and CH^{3+}.

Table IV. Observed Rate Constants[a]

$[HClO_4]$, M	$10^{-2}k_{obsd}^{vf}$, s^{-1}, (σ) (N)[b]	k_{obsd}^{f}, s^{-1}, (σ) (N)[b]	$10^{2}k_{obsd}^{s}$, s^{-1}, (σ) (N)[b]	$10^{3}k_{obsd}^{vs}$, s^{-1}, (σ) (N)[b]
0.0307		3.0 (0.2) (4)	0.8 (0.3) (3)	
0.0502	2.7 (0.2) (5)	4.0 (0.1) (4)		
0.0600		3.5 (0.1) (3)		
0.0697		3.3 (0.1) (3)	1.7 (0.2) (3)	
0.0892		3.9 (0.1) (3)		
0.109	2.8 (0.3) (4)	5.3 (0.1) (6)	3.8 (0.1) (1)	2.15 (0.03) (1)
0.128	2.8 (0.3) (7)	5.6 (0.1) (6)	4.0 (0.1) (4)	2.1 (0.4) (4)
0.148		5.9 (0.2) (12)	4.8 (0.2) (3)	2.6 (0.6) (3)
0.167	2.7 (0.2) (5)	6.5 (0.5) (13)	5.3 (0.5) (3)	2.6 (0.5) (3)
0.187		6.8 (0.6) (8)	6.2 (0.5) (8)	2.4 (0.3) (4)
0.226		7.3 (0.5) (7)	8.1 (0.5) (2)	
0.275	3.1 (0.1) (5)	8.7 (0.4) (7)	7.9 (0.3) (3)	
0.323	3.0 (0.2) (7)	9.2 (0.5) (7)		
0.362	3.2 (0.3) (4)	9.4 (0.5) (9)		
0.421		10.8 (0.6) (5)	8.6 (0.3) (4)	3.0 (0.1) (4)
0.518	3.2 (0.1) (4)	10.8 (0.7) (6)	9.6 (0.5) (4)	3.23 (0.04) (3)
0.616	3.2 (0.3) (5)	11.0 (0.9) (7)	11.5 (0.5) (4)	3.5 (0.1) (5)
0.713	3.1 (0.2) (7)	11.6 (1.2) (8)	12.0 (0.7) (3)	3.2 (0.1) (4)
0.811	3.0 (0.2) (5)	11.3 (0.3) (4)	11.4 (0.5) (4)	3.93 (0.09) (4)
0.908	2.8 (0.3) (6)	10.6 (0.9) (6)	11.3 (0.6) (4)	3.89 (0.09) (3)
1.01	2.9 (0.2) (8)	10.5 (0.3) (4)	12.2 (0.5) (3)	3.89 (0.06) (4)

[a] k_{obsd}^{x} represents the observed first-order rate constant for the first (x = vf), second (x = f), third (x = s), and final (x = vs) step of the ferrioxamine B aquation reaction. Conditions: 25.0 °C; I = 2.00 ($NaClO_4/HClO_4$); $[Fe(HDFB)^+]_{tot} = 2.90 \times 10^{-4}$ M. [b] σ = standard deviation; N = number of determinations.

Scheme I. Time-Dependent Equilibrium Scheme for Ferrioxamine B Aquation in Acidic Aqueous Solution

reaction designation	equilibrium scheme	equilibrium quotient[a]	molar absorbtivity,[a] M^{-1} cm^{-1}
vs, f	$A^+ + H^+ \rightleftharpoons BH^{2+}$	$K_1K_2 = 3.6$ (0.3) M^{-1} [c]	$\epsilon_A = \begin{cases} 2460\ (30)^b \\ 2540\ (20)^c \\ 2620\ (50)^d \end{cases}$
f, s	$BH^{2+} \rightleftharpoons C^{2+}$	$K_3 = 2.1$ (0.4)[d]	$\epsilon_{BH} = 1390$ (150)[c]
s, vs	$C^{2+} + H^+ \rightleftharpoons CH^{3+}$	$K_4'K_4 = 3.4$ (0.9) M^{-1} [e]	$\epsilon_C = \begin{cases} 1500^d \\ 2400^e \end{cases}$
vs	$CH^{3+} + H^+ \rightleftharpoons D^{3+} + E^+$	$K_5 = 8 \times 10^{-3}$ [f]	$\epsilon_{CH} = 1020$ (250)[e]

[a] Values in parentheses are uncertainties obtained from standard deviations of the parameters obtained from a nonlinear least-squares analysis using equations in the text as noted. [b] Directly observed from static measurements at pH >3. [c] Calculated using eq 3 and data obtained from the very fast reaction. [d] Calculated using eq 5 and data obtained from the fast reaction. [e] Calculated using eq 7 and data obtained from the slow reaction. [f] Calculated using eq 11 and data obtained from the very slow reaction.

1.0. Lastly, the fact that A_∞^{vs}/C_T does not decrease to zero at high $[H^+]$ indicates that, at our conditions (up to 1 M $HClO_4$), complete dissociation of ferrioxamine B into Fe_{aq}^{3+} and H_4DFB^+ does not occur.

Initial rates of ferrioxamine B aquation (fast reaction) as a function of the total ferrioxamine B concentration show the reaction to be first order in complex (see Table III).[31] The first-order rate constants for all four observable reactions as a function of $[H^+]$ at 25.0 °C, I = 2.0, are given in Table IV. These data are plotted in Figures 5–8.

Discussion

I. Equilibrium Studies. As Figure 3 indicates, there are five observable potential-energy minima in the aquation reaction of ferrioxamine B in acidic, aqueous solution. Therefore, there are a minimum of four equilibria to resolve. These will be resolved initially by using symbols A–E to represent reactants, products, and intermediates. Later, correlations will be made between each symbol and probable chemical species.

Equilibrium Scheme after Very Fast Reaction. The $[H^+]$ dependence of A_∞^{vf}/C_T at 425 nm is shown in Figure 3. The predominant trend in the data is a gradual decrease in A_∞^{vf}/C_T with increasing $[H^+]$. At the higher $[H^+]$ values, A_∞^{vf}/C_T becomes almost constant at a value of about 1600 M^{-1} cm^{-1}. This suggests that a more intensly colored species, A^+, is being converted by protonation to a less intensly colored species, BH^{2+}, as shown in reaction 2. The symbol A^+ represents ferrioxamine B (Fe-

$$A^+ + H^+ \rightleftharpoons BH^{2+} \qquad K_1K_2 \qquad (2)$$

(HDFB)$^+$, I). The chemical identity of BH^{2+} will be discussed later. Formulation of the equilibrium quotient for reaction 2 as the product of two equilibria (with equilibrium quotients K_1 and

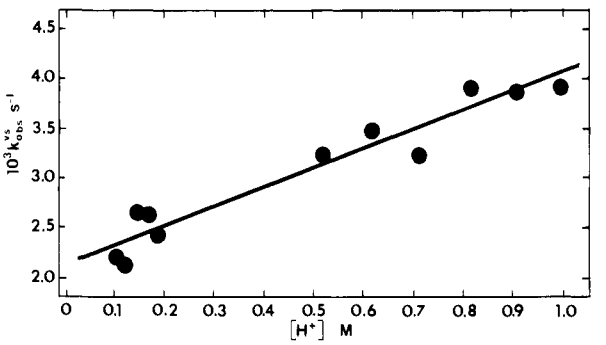

Figure 8. Observed first-order rate constants for the very slow reaction, k_{obsd}^{vs}, plotted as a function of $[H^+]$. Conditions are given in legend of Figure 5. Each data point represents 3–5 determinations. Data are from Table IV.

K_2) is based on kinetic data that are presented below. The $[H^+]$ dependence of A_∞^{vf}/C_T for reaction 2 may be expressed by eq 3.[32]

$$\frac{A_\infty^{vf}}{C_T} = \frac{\epsilon_A + \epsilon_{BH}K_1K_2[H^+]}{1 + K_1K_2[H^+]} \qquad (3)$$

A nonlinear least-squares fit of eq 3 to the data in Figure 3 yields the values for ϵ_A, ϵ_{BH}, and K_1K_2 given in Scheme I. These values and eq 3 were used to compute the solid line drawn through the A_∞^{vf}/C_T values in Figure 3. It is significant that the value for ϵ_A obtained from eq 3, 2540 (20) M^{-1} cm^{-1}, agrees with the molar absorptivity value observed for ferrioxamine B at pH 5 (ϵ = 2460 (30) M^{-1} cm^{-1}), where the complex is completely formed.

Equilibrium Scheme after Fast Reaction. A_∞^{f}/C_T has the $[H^+]$ dependence shown in Figure 3. One noticeable feature of this

plot is that A_∞^f/C_T becomes nearly independent of $[H^+]$ at high acidity. The $[H^+]$ independence of k_{obsd}^f at high $[H^+]$ (Figure 6, Table IV) suggests that a protonation equilibrium step occurs prior to the rate-determining step in the fast reaction (see below). Therefore, the simplest scheme consistent with these observations can be generated by merely adding reaction 4 to reaction 2.

$$BH^{2+} \rightleftharpoons C^{2+} \qquad K_3 \tag{4}$$

A_∞^f/C_T would then have the $[H^+]$ dependence given by eq 5.

$$\frac{A_\infty^f}{C_T} = \frac{\epsilon_A + (\epsilon_{BH} + \epsilon_C K_3)K_1K_2[H^+]}{1 + (1 + K_3)K_1K_2[H^+]} \tag{5}$$

Nonlinear least squares analysis of the data for A_∞^f/C_T in Figure 3 using eq 5 and the values obtained above for ϵ_{BH} and K_1K_2 yields values for ϵ_A, K_3, and ϵ_C (see Scheme I). The smooth curve drawn through A_∞^f/C_T values in Figure 3 was computed by using eq 5 and these parameters.

Equilibrium Scheme after Slow Reaction. A_∞^s/C_T is $[H^+]$ dependent even though A_∞^f/C_T is essentially independent of $[H^+]$ above 0.1 M (Figure 3). The simplest scheme consistent with this observation is to add reaction 6 to reaction 4, where reaction 6 would account for the $[H^+]$ dependence of A_∞^s/C_T. The reason for expressing the equilibrium quotient for reaction 6 as the

$$C^{2+} + H^+ \rightleftharpoons CH^{3+} \qquad K_4'K_4 \tag{6}$$

product $K_4'K_4$ is based on kinetic data to be discussed below. Consideration of reactions 4 and 6 allows derivation of eq 7 for the $[H^+]$ dependence of A_∞^s/C_T. Nonlinear least-squares analysis

$$\frac{A_\infty^s}{C_T} = \frac{\dfrac{\epsilon_{BH} + \epsilon_C K_3}{1 + K_3} + \left[\dfrac{\epsilon_{CH}K_3K_4'K_4}{1 + K_3}\right][H^+]}{1 + \dfrac{K_3K_4'K_4}{1 + K_3}[H^+]} \tag{7}$$

of the A_∞^s/C_T data using eq 7 and the values obtained above for ϵ_{BH} and K_3 yields the values for ϵ_{CH}, ϵ_C, and $K_4'K_4$ given in Scheme I. The smooth curve drawn through the A_∞^s/C_T data in Figure 3 was computed by using eq 7 and these parameters. The value of 1020 M^{-1} cm^{-1} for ϵ_{CH} is reasonable assuming that the symbol CH^{3+} represents ferrioxamine B after it has been doubly protonated (reactions 2 and 6). Since previous studies[24] have indicated that the molar absorbtivities of mono(hydroxamato)iron(III) complexes are all about 1000 ± 300 M^{-1} cm^{-1}, the simplest interpretation then would be that CH^{3+} contains only one hydroxamate chelate ring bound to iron(III).

Equilibrium Scheme after Very Slow Reaction. Positive equilibrium quotients could not be obtained when the data for A_∞^{vs}/C_T (Figure 3) were analyzed with a scheme corresponding to reactions 2, 4, and 6, or 4 and 6, and an $[H^+]$-independent equation. A scheme composed of reactions 4, 6, and 8 yields eq 9 for the $[H^+]$ dependence of A_∞^{vs}/C_T.

$$CH^{3+} + H^+ \rightleftharpoons D'^{4+} \qquad K_5' \tag{8}$$

$$\frac{A_\infty^{vs}}{C_T} = \frac{\dfrac{\epsilon_{BH} + \epsilon_C K_3}{1 + K_3} + \dfrac{\epsilon_{CH}K_3K_4'K_4}{1 + K_3}[H^+] + \dfrac{\epsilon_D K_3K_4'K_4K_5'}{1 + K_3}[H^+]^2}{1 + \dfrac{K_3K_4K_4'}{1 + K_3}[H^+] + \dfrac{K_3K_4K_4'K_5'}{1 + K_3}[H^+]^2} \tag{9}$$

A nonlinear least-squares fit of eq 9 to the A_∞^{vs}/C_T data in Figure 3 yielded a value of 50 ± 200 for ϵ_D. In the context of intensely colored iron(III) hydroxamic acid complexes, this can be interpreted to mean that the products of the very slow reaction do not absorb light at 425 nm. The most reasonable assignment then is that the products of the very slow reaction are Fe_{aq}^{3+} and the free ligand, H_4DFB^+. These species are represented as D^{3+} and E^+, respectively, in reaction 10, which, when considered with

$$CH^{3+} + H^+ \rightleftharpoons D^{3+} + E^+ \qquad K_5 \tag{10}$$

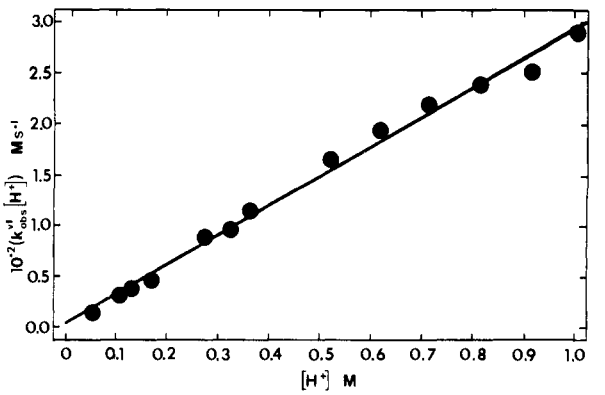

Figure 9. Plot of data shown in Figure 5 according to eq 15; see text.

reactions 4 and 6, constitutes the equilibria present for the very slow reaction. This analysis yields eq 11 for the $[H^+]$ dependence

$$\frac{A_\infty^{vs}}{C_T} = \left\{\frac{(\epsilon_{BH} + \epsilon_C K_3)K_3K_4^2K_4'^2K_5^3[H^+]^5}{1 + K_3} + \frac{\epsilon_{CH}K_3^2K_4^3K_4'^3K_5^3[H^+]^6}{1 + K_3}\left[\tfrac{1}{2} - \left(\tfrac{1}{4} + \frac{C_T}{K_3K_4^2K_4'^2K_5^3[H^+]^3}\right)^{1/2}\right]^2\right\} \Big/ \left\{1 + \frac{K_3K_4K_4'}{1 + K_3}[H^+]\right\} \tag{11}$$

of A_∞^{vs}/C_T. A nonlinear least-squares analysis of the A_∞^{vs}/C_T data (Figure 3) using eq 11 and the values obtained above for ϵ_{BH}, ϵ_C, K_3, and $K_4'K_4$ yields a value of 8×10^{-3} for K_5. This is a very reasonable value for the dissociation quotient of a mono(hydroxamato)iron(III) complex.[24]

Scheme I summarizes the results of the above discussion, with symbols representing chemical species. It also demonstrates the extent of overlap of the equilibria involved in the five potential-energy minima present in the path toward complete aquation of ferrioxamine B in acidic aqueous solution.

II. Kinetics. Very Fast Reaction. Reaction 2 is adequate to explain the $[H^+]$ dependence of A_∞^{vf}/C_T shown in Figure 3. However, treatment of reaction 2 as a one-step process is not consistent with the $[H^+]$ independence of k_{obsd}^{vf} shown in Figure 5.[33] A mechanism for the very fast reaction that is consistent with the available data is given by reactions 12 and 13, the sum

$$A^+ \rightleftharpoons B^+ \qquad k_1/k_{-1} \tag{12}$$

$$B^+ + H^+ \rightleftharpoons BH^{2+} \qquad K_2 \tag{13}$$

of which is represented by reaction 2. Assuming this to be a relaxation process, that $[B^+] \ll C_T$, and that proton transfer reaction 13 is in rapid equilibrium throughout, eq 14 may be derived. For reactions 12 and 13 to represent the correct

$$k_{obsd}^{vf} = k_1 + \frac{k_{-1}}{K_2[H^+]} \tag{14}$$

mechanism for the very fast reaction, it must be true that $k_1 \gg$

(33) Treating reaction 2 as a relaxation process gives eq 24, where k_f and

$$k_{obsd}^{vf} = k_f[H^+] + k_r \tag{24}$$

k_r are the microscopic rate constants in the forward and reverse direction, respectively. The invariance of k_{obsd}^{vf} with $[H^+]$ (Figure 5) requires that if reaction 2 represents the mechanism for this first step, then, according to eq 24, $k_f[H^+] \ll k_r = 290$ (30) s^{-1}. However, this mechanism can be ruled out on the basis of the following argument. Analysis of the equilibrium data for reaction 2 gave 3.6 (0.3) M^{-1} as the reaction quotient and therefore the ratio k_f/k_r. This yields $k_f = (3.6\ M^{-1})(290\ s^{-1}) = 1044\ M^{-1}\ s^{-1}$. According to this, $k_f[H^+]$ should range from 525 to 1044 s^{-1}. This is inconsistent with the assumption that $k_f[H^+] \ll k_r$ and, therefore, demonstrates that reaction 2 cannot represent the mechanism for the very fast reaction.

Scheme II. Reaction Scheme Based on Kinetic Data for Ferrioxamine B Aquation in Aqueous Solution

reaction designation	reaction steps		parameter values[a]
vf, f	$A^+ \rightleftharpoons B^+$	$K_1, k_1/k_{-1}$	$k_1 = 2.9\ (0.1) \times 10^2\ s^{-1}$ [b]
	$B^+ + H^+ \rightleftharpoons BH^{2+}$	K_2	$k_{-1}/K_2 < 10\ M^{-1}\ s^{-1}$ [b]
			$K_1K_2 = 5.2\ (1.4)\ M^{-1}$ [c]
s	$BH^{2+} \rightleftharpoons C^{2+}$	k_3/k_{-3}	$k_3 = 14\ (5)\ s^{-1}$ [c]
			$k_{-3} < 3\ s^{-1}$ [c]
	$C^{2+} + H^+ \rightleftharpoons C'H^{3+}$	K_4'	$K_4' < 0.4\ M^{-1}$ [d]
	$C'H^{3+} \rightleftharpoons CH^{3+}$	k_4/k_{-4}	$k_4 = 1.8\ (0.2) \times 10^{-1}\ s^{-1}$ [e]
			$k_{-4} \leq 5 \times 10^{-3}\ s^{-1}$ [f]
vs	$CH^{3+} + H^+ \rightleftharpoons D^{3+} + E^+$	k_5/k_{-5}	$k_5 = 1.9\ (0.2) \times 10^{-3}\ M^{-1}\ s^{-1}$ [g]
	$\rightleftharpoons$ ($-H^+ \Downarrow H^+$)		$k_{-5} = 2 \times 10^{-1}\ M^{-1}\ s^{-1}$ [h]
	$D(OH)^{2+} + E^+$	k_6/k_{-6}	$k_6 = 2.1\ (0.1) \times 10^{-3}\ s^{-1}$ [g]
			$k_{-6} = 2 \times 10^2\ M^{-1}\ s^{-1}$ [i]

[a] Values in parentheses are uncertainties obtained from standard deviations of the parameters obtained from a nonlinear least-squares analysis using equations in the text as noted. [b] Value computed from eq 15, which was derived assuming reaction 13 to be in rapid equilibrium and $[B^+] \ll C_T$. [c] Value computed from eq 17, which was derived assuming a relaxation process for reactions 2 and 16 and $[B^+] \ll C_T$. [d] Value computed from eq 20 by using a value for K_3 calculated from the ratio k_3/k_{-3} obtained from a kinetic analysis of the fast reaction. [e] Value computed from eq 20. [f] Value obtained from Figure 7 and eq 20; see text. [g] Value obtained from eq 23. [h] Value computed from the ratio k_5/K_5. [i] Value computed from K_5, k_6, and the literature value (ref 34) for the hydrolysis constant for $Fe(H_2O)_6^{3+}$.

$k_{-1}/(K_2[H^+])$ (due to the observed invariance of k_{obsd}^{vf} with respect to $[H^+]$; see Figure 5). Equation 14 was rearranged to eq 15,

$$k_{obsd}^{vf}[H^+] = k_1[H^+] + k_{-1}/K_2 \qquad (15)$$

and a plot of the data according to the later equation is shown in Figure 9. This analysis yields $k_1 = 294\ (8)\ s^{-1}$ and $k_{-1}/K_2 < 10\ M^{-1}\ s^{-1}$. This is consistent with the inequality $k_1 \gg k_{-1}/(K_2[H^+])$ and establishes reactions 12 and 13 as valid mechanistic steps for the initial very fast reaction. This result is summarized in Scheme II.

Fast Reaction. The data listed in Table IV and plotted in Figure 6 demonstrate that k_{obsd}^{f} varies with $[H^+]$ until a plateau value of 10.9 (0.4) s^{-1} at high $[H^+]$ is reached. A mechanism consistent with these data is given by reactions 2 (sum of reactions 12 and 13) and 16.

$$A^+ + H^+ \rightleftharpoons BH^{2+} \qquad K_1K_2 \qquad (2)$$

$$BH^{2+} \rightleftharpoons C^{2+} \qquad k_3/k_{-3} \qquad (16)$$

Assuming the intermediate species, B^+ (reaction 12), is only present at low levels and treating the reaction as a relaxation process yield eq 17 for the $[H^+]$ dependence of k_{obsd}^{f}. Equation

$$k_{obsd}^{f} = \frac{k_3K_1K_2[H^+]}{1 + K_1K_2[H^+]} + k_{-3} \qquad (17)$$

17 was fitted to the data in Figure 6 by using a nonlinear least-squares technique. This analysis produced values for k_3 and K_1K_2 and a maximum value for k_{-3}. These are given in Scheme II. The solid curve drawn through the data points in Figure 6 was computed by using these parameters and eq 17. The value $k_3 = 14\ (5)\ s^{-1}$ obtained from eq 17 is in reasonable agreement with the plateau values shown in Figure 6 for k_{obsd}^{f} at high $[H^+]$. Also, this value for k_3 and the maximum value for k_{-3} ($<3\ s^{-1}$) are in reasonble agreement, within experimental error, with the value for K_3 (Scheme I) obtained from an analysis of the equilibrium data.

Slow Reaction. The data in Table IV that are plotted in Figure 7 demonstrate that k_{obsd}^{s} also becomes independent of $[H^+]$ at high $[H^+]$. This behavior suggests that a rapid proton-transfer step preceeds the rate-determining step and necessitates expressing reaction 6 from equilibrium Scheme I as the sum of two reactions (reactions 18 and 19). Reaction 16 is included in the scheme

$$BH^{2+} \rightleftharpoons C^{2+} \qquad K_3 \qquad (16)$$

$$H^+ + C^{2+} \rightleftharpoons C'H^{3+} \qquad K_4' \qquad (18)$$

$$C'H^{3+} \rightleftharpoons CH^{3+} \qquad k_4/k_{-4} \qquad (19)$$

for the slow reaction since BH^{2+} is still a major species, as indicated by the convergence of the A_∞ values for the fast, slow, and very slow reactions at low $[H^+]$ (Figure 3). Since BH^{2+} and C^{2+} are indistinguishable due to similar molar absorbtivities, K_3 and K_4' may be combined in the mathematical treatment of the proposed

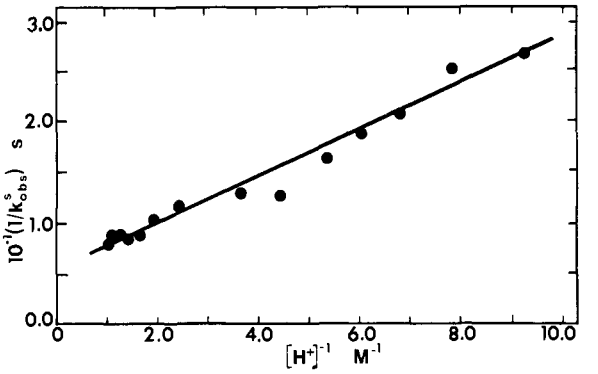

Figure 10. Plot of data shown in Figure 7 according to eq 21; see text.

mechanism for the slow reaction in order to derive an expression for k_{obsd}^{s}. Treating this proposed mechanism as a relaxation process yields eq 20 for the $[H^+]$ dependence of k_{obsd}^{s}. Consid-

$$k_{obsd}^{s} = \frac{k_4K_3K_4'[H^+]}{1 + K_3K_4'[H^+]} + k_{-4} \qquad (20)$$

eration of the data plotted in Figure 7 suggests that $k_{-4} \leq 0.005\ s^{-1}$. Confirmation that k_{-4} does not significantly contribute to k_{obsd}^{s} may be obtained from a plot of $1/k_{obsd}^{s}$ vs. $1/[H^+]$, which is linear (Figure 10). This linear behavior is expected if we set $k_{-4} = 0$ and rearrange eq 20 to eq 21. A nonlinear least-squares fit of

$$\frac{1}{k_{obsd}^{s}} = \frac{1}{k_4} + \frac{1}{k_4K_3K_4'}\left(\frac{1}{[H^+]}\right) \qquad (21)$$

eq 20 to the data in Figure 7, assuming a negligible contribution from the k_{-4} term, yields the value for k_4 given in Scheme II. By considering K_3 as the ratio of rate constants k_3/k_{-3} obtained from the kinetic analysis of the fast reaction, the upper limit for K_4' listed in Scheme II may also be obtained from this kinetic analysis of the slow reaction.

Very Slow Reaction. The data in Table IV that are plotted in Figure 8 demonstrate the influence of $[H^+]$ on k_{obsd}^{vs}. Equation 22 adequately describes these data. Reaction 23 represents a

$$k_{obsd}^{vs} = k_5[H^+] + k_6 \qquad (22)$$

$$CH^{3+} + H^+ \rightleftharpoons D^{3+} + E^+ \qquad k_5/k_{-5}$$
$$\rightleftharpoons \quad (H^+ \Downarrow -H^+) \qquad (23)$$
$$D(OH)^{2+} + E^+ \qquad k_6/k_{-6}$$

proposed mechanism for this final stage of ferrioxamine B aquation and corresponds to the addition of a parallel aquation path to reaction 10 in the equilibrium data analysis (Scheme I). Equation 22 may be derived by assuming reaction 23 is a relaxation process[24]

Scheme III

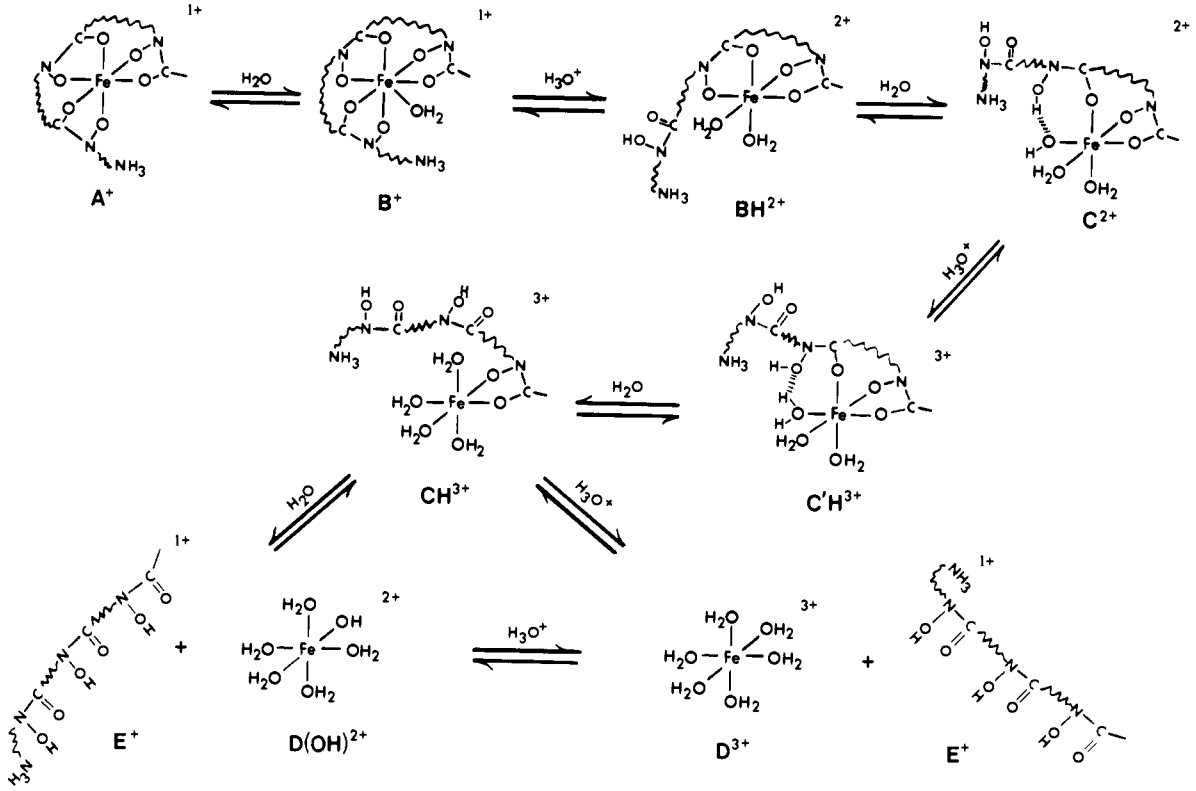

and recognizing that the reverse-reaction rate constants (complex formation k_{-5}, k_{-6}) are not observable, since at low [H^+], where these terms would predominate, other reactions occur in the ferrioxamine B system (further complex formation or ring closure). Values for k_5 and k_6 are obtained from a linear least-squares analysis of the data shown in Figure 8 and are listed in Scheme II. Additional confirmation of the validity of this mechanism (reaction 23) comes from the analysis of the equilibrium absorbance data, which yields a value of 8×10^{-3} for K_5. Assuming D^{3+} and E^+ to be $Fe(H_2O)_6^{3+}$ and H_4DFB^+, respectively (see above), and using literature data for the hydrolysis constant for iron,[34] we can use K_5, k_5, and k_6 to compute k_{-5} and k_{-6} as 2×10^{-1} and 2×10^2 M^{-1} s^{-1}, respectively. These are reasonable values for second-order rate constants for hydroxamic acid ligand substitution at $Fe(H_2O)_6^{3+}$ and $Fe(H_2O)_5OH^{2+}$.[24]

III. Overall Mechanism. Nine species (A^+, B^+, BH^{2+}, C^{2+}, $C'H^{3+}$, CH^{3+}, D^{3+}, $D(OH)^{2+}$, and E^+) have been proposed as starting materials, intermediates, and products in the aquation reaction of ferrioxamine B over the [H^+] range investigated. These species are necessary to account for the equilibrium spectral changes, kinetic results, and overall reaction stoichiometry with respect to H_{aq}^+. The reaction scheme developed from an analysis of the kinetic data (Scheme II) is consistent with that obtained from the equilibrium spectral changes (Scheme I). The proposed structures of these species and their interconversions are shown in Scheme III. In developing the pictorial view presented in Scheme III, certain assumptions based on analogy with similar systems have been made. The assumption that these intermediate species represent a partially unwrapped siderophore ligand is reasonable on the basis of observed spectral changes and evidence that the bidentate segments of similar polydentate ligand systems can act relatively independent of each other.[35] Hence, it is not unreasonable to view the aquation of ferrioxamine B as occurring in steps similar to the dissociation of a tris(hydroxamato)iron(III) complex.

The unwrapping process is shown in Scheme III to begin at the protonated amine end of the molecule. This appears reasonable by analogy to our previous kinetic studies of synthetic monohydroxamic acid complexes of iron(III), where we have shown that dissociation of a hydroxamate chelate group occurs initially at the N–O oxygen atom, followed by carbonyl oxygen atom dissociation from the inner coordination shell of iron(III).[24] This then requires the dissociation process to be initiated at the protonated amine end of the ligand, since to propose otherwise would mean either that a carbonyl oxygen atom is first to dissociate or that dissociation must be initiated at a nonterminus point in the linear ligand. (Furthermore, it is not unreasonable that dissociation would be initiated nearest the site of ligand protonation.) It is reasonable then that the second, third, etc., oxygen atom dissociation from iron(III) proceeds sequentially down the linear hydroxamate chain as shown in Scheme III.

The starting material, A^+, is represented as the protonated amine hexadentate complex (I) on the basis of its spectral properties and previously published work.[10] Evidence for BH^{2+} comes from both kinetic and equilibrium (spectral) analyses of the data, including the stoichiometric requirement of one proton. The structure shown in Scheme III for BH^{2+} is supported by its visible absorption spectrum, which is consistent with that for two bound hydroxamate groups. Furthermore, the formation quotient (K_1K_2) for BH^{2+} was obtained from both kinetic and equilibrium data and is consistent with the literature constant for the formation of tetradentate ferrioxamine B from the protonated hexadentate complex.[10,36]

(34) Milburn, R. M. *J. Am. Chem. Soc.* **1957**, *79*, 537.
(35) See, for example: Carrano, C. J.; Cooper, S. R.; Raymond, K. N. *J. Am. Chem. Soc.* **1979**, *101*, 599.

(36) Schwarzenbach[10] reports log $K = 0.94$ for the equilibrium constant for formation of tetradentate ferrioxamine B (BH^{2+} in Scheme III) from the protonated hexadentate species (A^+ in Scheme III) at 20 °C, $I = 0.1$. This is slightly larger than the value we have determined. However, Schwarzenbach's result is based on static measurements over the pH range from 4 to 1. At the lower end of this range, our results indicate that additional dissociation reactions are beginning to occur that were not accounted for in Schwarzenbach's analysis. Our dynamic measurements do take subsequent protonation/dissociation equilibria into account, and consequently, the log $K_1K_2 = 0.72$ value based on the kinetic data reported here may be more accurate for the $A^+ + H^+ \rightleftharpoons BH^{2+}$ equilibrium at 25 °C, $I = 2.0$.

Evidence for the existence of some B^+ species intermediate between fully bound ferrioxamine B (A^+) and a tetradentate form (BH^{2+}) comes solely from the kinetic analysis of the very fast reaction. This species can only be present as a minor component. Since B^+ is an intermediate between A^+ and BH^{2+}, reasonable structures for this species are limited. The proposed structure shown in Scheme III involves addition of a coordinated water. Justification for this structure comes from our previously reported recognition of the importance of a coordinated H_2O cis to the dissociating hydroxamate functional group[24] and the fact that seven-coordinate iron(III) complexes are known.[37] Species B^+ may also include some H-bonding interaction between coordinated H_2O and the dissociating hydroxamate oxygen atom, as shown in structure C^{2+} for the second hydroxamate dissociation.

Species CH^{3+} is shown in Scheme III as having only one hydroxamate group bound to iron(III). This assignment is based on the visible absorption spectrum of CH^{3+},[38] which is comparable to that observed for mono(hydroxamato)iron(III) complexes,[24] and the observation that D^{3+} and E^+ do not absorb light in the visible region of the spectrum and therefore are assigned to $Fe(H_2O)_6^{3+}$ and H_4DFB^+, respectively. Further support of this structure for CH^{3+} comes from the acid-dependent (k_5) and acid-independent (k_6) rate constants for the conversion of CH^{3+} to D^{3+} and E^+, which are comparable to the corresponding rate constants for mono(hydroxamato)iron(III) aquation.[24]

Species C^{2+} and $C'H^{3+}$ represent two intermediates that occur between tetradentate- (BH^{2+}) and bidentate- (CH^{3+}) coordinated ferrioxamine B and that differ from each other by a proton. Within these limitations, the half-dissociated ligand species differing by a H-bonded proton, which are shown in Scheme III, are reasonable structures.

The first-order rate constants for the dissociation of successive hydroxamate groups from ferrioxamine B vary by a factor of 10^5, with dissociation of the last hydroxamate group being the slowest. Since each dissociating group is a similar hydroxamate moiety that is being replaced by H_2O ligands and since the chain length between hydroxamate groups is reasonably long, steric factors should be relatively small. This observation illustrates the significant difference in labilizing effect between coordinated H_2O and $-C(O)-N(O^-)-$. This may be due to differences in coordinating ability as well as net charge at the metal center.

The final step of ferrioxamine B aquation proceeds by two parallel paths (reaction 23; Scheme III), which is typical of many iron(III) aquation processes in aqueous solution. Comparison of k_5 and k_6 to the corresponding constants for mono(hydroxamato)iron(III) complexes shows that both acid-dependent and acid-independent aquation rate constants are smaller for ferrioxamine B than for the synthetic hydroxamic acids investigated in our laboratory.[14,24] *Thus, the natural product deferriferrioxamine B has a structure that minimizes the aquation rate of ferrioxamine B by both acid-dependent and acid-independent paths to enhance both the thermodynamic and kinetic stability of the iron complex.* The rate constants and equilibrium constant for the final step of the aquation reaction, and the literature value for the $Fe(H_2O)_6^{3+}$ hydrolysis constant,[34] allow us to compute values for the rate constants of the ferrioxamine B formation reaction. The computed rate constants for reaction with $Fe(H_2O)_6^{3+}$ and $Fe(H_2O)_5OH^{2+}$ at 25 °C, $I = 2.0$, are 2×10^{-1} M^{-1} s^{-1} and 2×10^2 M^{-1} s^{-1}, respectively. These formation rate constants are a factor of 4–20 smaller than the corresponding formation rate constants for the synthetic monohydroxamic acids[24] but are consistent with the trends established by them. These data taken in total suggest a variable degree of hydroxamic acid ligand participation in the transition state, which is consistent with the associative-interchange character previously proposed for the mono(hydroxamato)iron(III)-formation reactions.[24] However, it is possible that charge and/or steric effects may also influence the kinetics of ferrioxamine B complex formation.

Acknowledgment. **Acknowledgment** is made to the donors of the Petroleum Research Fund, administered by the American Chemical Society, for support of this research. We also thank the Ciba Geigy Corporation for their generous gift of the methanesulfonate salt of deferriferrioxamine B (DESFERAL).

Registry No. $[Fe(HDFB)]ClO_4$, 82265-74-5; $(H_3DFB)MeSO_3H$, 138-14-7; $Fe(HDFB)^+$, 82265-75-6; Fe, 7439-89-6.

Supplementary Material Available: Absorbance and rate data, Tables I–III (4 pages). Ordering information is given on any current masthead page.

(37) See, for example: Spijkermann, J. J.; Hall, L. H.; Lambert, J. L. *J. Am. Chem. Soc.* **1968**, *90*, 2039.

(38) The inset of Figure 3 shows that CH^{3+} has a $\lambda_{max} \sim 480$ nm; $\epsilon_{CH} = 1020$ (250) M^{-1} cm^{-1} at 425 nm from dynamic-equilibrium measurements (Scheme I).

Treflorine, Trenudine, and *N*-Methyltrenudone: Novel Maytansinoid Tumor Inhibitors Containing Two Fused Macrocyclic Rings

Richard G. Powell,*† David Weisleder,† Cecil R. Smith, Jr.,† John Kozlowski,‡ and William K. Rohwedder†

Contribution from the Northern Regional Research Center, Agricultural Research Service, U.S. Department of Agriculture, Peoria, Illinois 61604, and Department of Medicinal Chemistry and Pharmacognosy, Purdue University, West Lafayette, Indiana 47907. *Received February 1, 1982*

Abstract: Treflorine ($C_{36}H_{48}ClN_3O_{12}$), trenudine ($C_{36}H_{48}ClN_3O_{13}$), and *N*-methyltrenudone ($C_{37}H_{48}ClN_3O_{13}$), isolated from *Trewia nudiflora* (Euphorbiaceae) seed, are the first representatives of a new class of maytansinoid tumor inhibitors containing two fused macrocyclic rings. In addition to the 19-membered ring characteristic of all previously known maytansinoids, these new compounds have a 12-membered ring joining C-3 and the amide nitrogen at C-18. The structures of these new maytansinoids were established by 470-MHz ^1H NMR, ^{13}C NMR, and mass spectrometry and chemical degradation.

The seed of *Trewia nudiflora* L. (Euphorbiaceae), a tree native to parts of India, is a rich source of maytansinoids including trewiasine (**1**), dehydrotrewiasine (**2**), and demethyltrewiasine (**3**).[1] There is considerable current interest in maytansinoids because of their unique ansa macrolide structure together with their exceptionally potent antitumor activity[2] and a range of other bio-

†Northern Regional Research Center.
‡Purdue University.

(1) Powell, R. G.; Weisleder, D.; Smith, C. R., Jr. *J. Org. Chem.* **1981**, *46*, 4398–4403.